Martinus Nijhoff/Dr. W. Junk, The Hague.
Tamura, N., & Cheniae, G. (1987a) *Biochim. Biophys. Acta 890*, 179-194.
Tamura, N., & Cheniae, G. (1987b) in *Progress in Photosynthesis Research* (Biggins, J., Ed.) Vol. 1, pp 621-624, Martinus Nijhoff, Dordrecht.
Tamura, N., & Cheniae, G. M. (1988) in *Light-Energy Transduction in Photosynthesis: Higher Plant and Bacterial Models* (Stevens, S. E., Jr., & Bryant, D. A., Eds.) pp 227-242, The American Society of Plant Physiologists, Rockville, MD.
Tamura, N., Inoue, Y., & Cheniae, G. M. (1989) *Biochim. Biophys. Acta 976*, 173-181.
Tanaka-Kitatani, Y., Satoh, K., & Katoh, S. (1990) *Plant Cell Physiol. 31*, 1039-1047.
Yocum, C. F. (1980) *Methods Enzymol. 69*, 576-584.
Zimmermann, J.-L., & Rutherford, A. W. (1986) *Biochim. Biophys. Acta 851*, 416-423.

Using Saturation-Recovery EPR To Measure Distances in Proteins: Applications to Photosystem II†

Donald J. Hirsh, Warren F. Beck,‡ Jennifer B. Innes,§ and Gary W. Brudvig*
Department of Chemistry, Yale University, 225 Prospect Street, New Haven, Connecticut 06511
Received July 3, 1991; Revised Manuscript Received October 4, 1991

ABSTRACT: The stable tyrosine radical $Y_D^\bullet$ (tyrosine 160 in the D2 polypeptide) in photosystem II (PSII) exhibits nonexponential electron spin-lattice relaxation transients at low temperature. As previously reported, the tetranuclear Mn complex in PSII significantly enhances the spin-lattice relaxation of $Y_D^\bullet$. However, in Mn-depleted PSII membranes, the spin-lattice relaxation transients of $Y_D^\bullet$ are also nonexponential, and progressive power saturation ($P_{1/2}$) experiments show that it does not behave like an isolated tyrosine radical. A model is developed to treat the interaction of two paramagnets in a rigid lattice at a fixed distance apart but with a random orientation in a magnetic field. This model describes the spin-lattice relaxation of a radical in proximity to another paramagnetic site in terms of three relaxation rate constants: the "intrinsic" relaxation rate, the relaxation rate due to scalar exchange, and the relaxation rate due to dipole-dipole interactions. The intrinsic and the scalar exchange relaxation rates are isotropic and together contribute a single rate constant to the spin-lattice relaxation transients. However, the dipolar relaxation rate is orientation dependent. Each orientation contributes a different dipolar relaxation rate constant to the *net* spin-lattice relaxation rate constant. The result is a superposition of single-exponential recoveries, each with a different net rate constant, causing the observed saturation-recovery transients to be non-(single)-exponential. Saturation-recovery relaxation transients of $Y_D^\bullet$ are compared with those of a model tyrosine radical, generated by UV photolysis of L-tyrosine in a borate glass. From this comparison, we conclude that scalar exchange does not make a significant contribution to the spin-lattice relaxation of $Y_D^\bullet$ in Mn-depleted PSII. We account for the nonexponential relaxation transients obtained from $Y_D^\bullet$ in Mn-depleted PSII membranes in terms of dipolar-induced relaxation enhancement from the non-heme Fe(II). From simulations of the spin-lattice relaxation transients, we obtain the magnitude of the magnetic dipolar interaction between $Y_D^\bullet$ and the non-heme Fe(II), which can be used to calculate the distance between them. Using data on the non-heme Fe(II) in the reaction center of *Rhodobacter sphaeroides* to model the non-heme Fe(II) in PSII, we calculate a $Y_D^\bullet$-Fe(II) distance of $\geq$38 Å in PSII. This agrees well with the distance predicted from the structure of the bacterial reaction center.

Researchers have noted in several studies of multisite redox enzymes that a paramagnetic species of interest showed nonexponential (or at least non-single-exponential) spin-lattice (T_1) relaxation kinetics at temperatures under 100 K. Examples include Cu_A in cytochrome oxidase (Scholes et al., 1984) and the tyrosine radical $Y_D^\bullet$ in PSII[1] (Britt et al., 1987; Evelo et al., 1989; Beck et al., 1990). We suggest that in both cases the source of the observed nonexponential spin-lattice relaxation kinetics is an orientationally dependent dipole-dipole interaction between the observed spin system and one or more of the endogenous paramagnetic centers in these enzymes. In this paper, we demonstrate that the unusual spin-lattice relaxation kinetics of $Y_D^\bullet$ in manganese-depleted PSII arise directly from its dipolar interaction with another paramagnetic center, probably the non-heme Fe(II).

PSII contains a remarkably stable tyrosine radical, $Y_D^\bullet$, which exhibits the well-studied EPR spectrum known as signal II_s (Babcock et al., 1989). Although it is now known that $Y_D^\bullet$ is located at tyrosine 160 in the D2 polypeptide (Debus et al., 1988; Vermaas et al., 1988), the location of Y_D with respect to the other components of the O_2-evolving center (OEC) and to the rest of the PSII reaction center is not well established.

† This research was supported by the National Institutes of Health (GM36442).
‡ Current address: Department of Chemistry, Vanderbilt University, Nashville, TN 37235.
§ Current address: Department of Chemistry, University of Connecticut, Storrs, CT 06269.

[1] Abbreviations: Chl, chlorophyll; EPR, electron paramagnetic resonance; HEPES, *N*-(2-hydroxyethyl)-piperazine-*N*'-2-ethanesulfonic acid; MES, 2-(*N*-morpholino)ethanesulfonic acid; OEC, O_2-evolving center; PSII, photosystem II; $Y_D^\bullet$, tyrosine radical in photosystem II giving rise to signal II_s.

0006-2960/92/0431-532$03.00/0 © 1992 American Chemical Society

If the sequence homology between the L and M subunits of the reaction center from *Rhodopseudomonas viridis* and the D1 and D2 subunits of PSII is an indication of structural homology, one can estimate the distance between $Y_D^\bullet$ and the non-heme Fe(II) (Michel & Deisenhofer, 1988). Tyrosine 160 (Y_D) of D2 corresponds to histidine 162 in the M subunit of the bacterial reaction center. The distance from the center of the imidazole ring of histidine 162 to the non-heme Fe(II) in *Rps. viridis* is 36.8 Å. However, there is currently no reliable estimate of this distance from direct measurements on PSII. The function of $Y_D^\bullet$ in the mechanism of photosynthetic water oxidation remains unclarified, but it is known that $Y_D^\bullet$ participates in the dark one-electron oxidation of the OEC from the S_0 to S_1 state (Styring & Rutherford, 1987).

The electron spin relaxation properties of $Y_D^\bullet$ have been studied in the past by continuous EPR power saturation (Warden et al., 1976; Hales & Das Gupta, 1981; Styring & Rutherford, 1988; Isogai et al., 1988; Innes & Brudvig, 1989) and electron spin echo techniques (Nishi et al., 1978; de Groot et al., 1986; Britt et al., 1987; Evelo et al., 1989; Evelo, 1990). In this work, we have employed the pulsed EPR method of saturation recovery (Hyde, 1979) to measure directly the electron spin-lattice relaxation properties of $Y_D^\bullet$ and also to characterize a model system employing photochemically generated and cryogenically trapped L-tyrosine radicals in a borate glass. The saturation-recovery transient records the recovery of the bulk z-magnetization to its equilibrium value in a static magnetic field. If all of the observed spins relax with the same time constant, the bulk magnetization will recover with single-exponential kinetics. If, however, a dipolar relaxation mechanism causes each spin to relax with a time constant that is a function of that spin's orientation, and the spins are randomly oriented in the sample, then the saturation-recovery transient will be the superposition of many single-exponential recoveries. The net result is a non-(single)-exponential recovery for the bulk magnetization. We proposed earlier that this was the explanation for the anomalous spin-lattice relaxation behavior of $Y_D^\bullet$ (Beck et al., 1990).

The same considerations apply to progressive power saturation ($P_{1/2}$) experiments. $P_{1/2}$, the microwave power at half-saturation, is proportional to $(H_{1/2})^2$, the microwave magnetic field needed to saturate a spin packet and defined by $(H_{1/2})^{1/2} = 1/(\gamma^2 T_1 T_2)$. If all of the observed spins relax with the same time constants, T_1 and T_2, then there should be a single $P_{1/2}$ value for a given instrumental and experimental configuration. If T_1 and T_2 are a function of the spin's orientation in the static magnetic field, then there will be a range of "$P_{1/2}$ values" in a randomly oriented matrix of spins.

We develop equations that describe the saturation-recovery transient of a "slow" relaxing spin when its spin-lattice relaxation is perturbed by pairwise interactions with a "fast" relaxing spin. These equations are general for the pairwise interaction of two paramagnetic centers and when applied to a saturation-recovery transient make it possible to seperate the orientation-dependent and isotropic contributions to the spin-lattice relaxation. We have applied them quantitatively to the case of the tyrosine radical $Y_D^\bullet$ in PSII. We also analyze the effect of dipole-dipole induced relaxation on $P_{1/2}$ measurements of $Y_D^\bullet$.

Materials and Methods

Sample Preparation. PSII membranes were isolated from market spinach leaves as previously described (Berthold et al., 1981; Beck et al., 1985). For storage at 77 K and for low-temperature EPR experiments, PSII membranes were suspended in a resuspension buffer: 20 mM MES, 15 mM NaCl, and 30% (v/v) ethylene glycol (as a cryoprotectant), pH 6.0. For studies involving the S_2 oxidation state of the Mn complex in the OEC, the S_2-state multiline EPR signal was generated in extensively dark-adapted S_1-state PSII membranes by a 2-min illumination at 210 K, as previously described (Beck et al., 1985).

The following method was used to deplete PSII of manganese. PSII membranes were suspended to 1 mg of Chl/mL in buffer A: 0.4 M sucrose, 50 mM MES, 15 mM NaCl, and 1 mM $CaCl_2$, pH 6.5. The presence of 0.4 M sucrose accelerates the release of Mn(II) ions. The suspension was mixed 1:1 with buffer A containing 10 mM NH_2OH and 10 mM EDTA and allowed to incubate for an hour at 0 °C. PSII membranes were pelleted by centrifugation and resuspended to a concentration of ≤0.3 mg of Chl/mL in buffer A containing 5 mM EDTA. This suspension was incubated for 10 min and centrifuged. The pellet was resuspended in buffer A and centrifuged again before finally suspending it in resuspension buffer. $Y_D^\bullet$ was generated in Mn-depleted samples by illuminating the sample with a quartz-halogen lamp (700 W/m^2) for 6 min in a transparent quartz Dewar filled with ice water followed by a 3-min dark incubation at 0 °C. For saturation-recovery experiments, the concentration of PSII was approximately 12 mg of Chl/mL. Experiments with anaerobic samples prepared on a vacuum system gave no indication that the measured electron spin-lattice relaxation rates were affected by ambient dissolved O_2.

L-Tyrosine was used as received from Aldrich. L-Tyrosine radicals (Sahlin et al., 1987) were generated in a frozen solution of 10 mM L-tyrosine in 12.5 mM sodium borate, pH 10. The radicals were generated by an 8-min illumination with a 250-W Hg arc lamp at 77 K.

The B2 subunit of ribonucleotide reductase from *Escherichia coli* was isolated as described previously (Beck et al., 1991). The EPR sample contained approximately 50 μM tyrosine radical in 25 mM HEPES, 10% ethylene glycol, pH 7.5.

Mn Assay. The Mn content of NH_2OH-treated PSII membranes was assayed by EPR. PSII membranes at 4.8 mg of Chl/mL were mixed 1:1 with 1 N HCl and incubated for an hour in an EPR tube. The $Mn(H_2O)_6^{2+}$ signal from denatured PSII was compared to an equal volume of a 5 μM $Mn(H_2O)_6^{2+}$ standard. The concentration of manganese in NH_2OH-treated PSII membranes was 0.17 ± 0.03 Mn/200 Chl.

EPR Measurements. Saturation-recovery EPR spectroscopy and conventional continuous-wave (cw) EPR spectroscopy were performed on a home-built X-band pulsed EPR spectrometer (Beck et al., 1991). Saturation-recovery transients were obtained with direct cw detection (without magnetic field or microwave frequency modulation) in the absorption mode. To nullify contributions from free induction decay (Hyde, 1979), the phase of the saturating pulses was set to 90° with respect to the continuous observing phase, and the phase of the saturating pulses was modulated every other pulse by a 180° phase modulator. The magnetic field was set at the zero crossing point of the first derivative spectrum (Figure 1, vertical arrows). The pumping microwave power level was usually set to 250–450 mW. Saturating pulse widths were set equal to either the T_1 (L-tyrosine) or $k_{1\text{scalar}}$ ($Y_D^\bullet$) of the sample at each temperature to saturate spin diffusion channels (Beck et al., 1991).

In a saturation-recovery experiment, the observing microwave power level, P, produces an isotropic relaxation en-

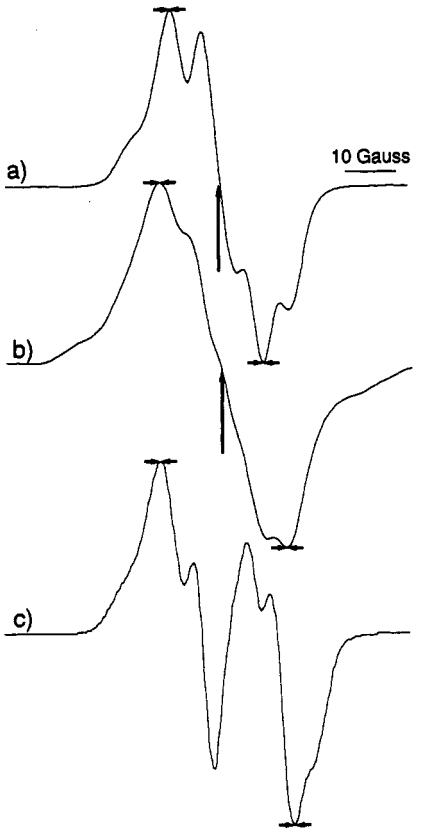

FIGURE 1: Continuous-wave first-derivative EPR spectra of (a) the stable tyrosine radical $Y_D^\bullet$ in spinach PSII membranes, (b) a UV-generated model L-tyrosine radical in a borate glass, and (c) the tyrosine radical of ribonucleotide reductase isolated from *E. coli*. Each spectrum was recorded with a 2.0-G field-modulation amplitude, 100-kHz field-modulation frequency, 9.05-GHz microwave frequency, and 720-nW microwave power. Spectra a and b were recorded at 5 K, spectrum c at 7 K. The vertical arrows mark the static magnetic field positions employed for the saturation–recovery measurements. The horizontal arrows mark the positions used to measure the peak-to-peak height in the spectra for the progressive power saturation ($P_{1/2}$) measurements.

hancement. We have shown previously for the inhomogeneously broadened line of the tyrosine radical of ribonucleotide reductase that the observed spin–lattice relaxation rate $1/T_1(P)$ is linearly dependent on P, for $P \ll P_{1/2}$ (Beck et al., 1991), that is

$$1/T_1(P) = 1/T_1 + CP \tag{1}$$

where $1/T_1$ is the limiting rate unperturbed by the observing microwave power level and C is a constant. The corresponding equation for the case where scalar exchange is also a source of relaxation enhancement is then

$$k_{1\text{scalar}}(P) = k_{1\text{scalar}} + C'P \tag{2}$$

where $k_{1\text{scalar}}$ is the sum of k_{1i} and k_{1ex} as described below under Theory. To determine $1/T_1$ or $k_{1\text{scalar}}$ at a given sample temperature, three to four saturation–recovery transients were recorded, each at a different level of observing microwave power. For the UV-generated tyrosine radical, each saturation–recovery transient was fit to a single exponential to determine $1/T_1(P)$. $1/T_1$ was determined by a linear least-squares fit of eq 1 to the $1/T_1(P)$'s. For $Y_D^\bullet$, each saturation–recovery transient was fit to the dipolar model (eqs 14 and 17) to determine $k_{1\text{scalar}}(P)$ and k_{1d} at that power level. $k_{1\text{scalar}}$ was then determined by a linear least-squares fit of eq 2 to the $k_{1\text{scalar}}(P)$'s. k_{1d} was taken as the average of the fitted values of k_{1d} since the observing microwave power should make no contribution to the orientationally dependent relaxation rate constant. The dipolar model (eqs 14 and 17) was fit by a nonlinear regression program that employed the Marquardt algorithm (Press et al., 1989). The integral in eq 14 was approximated by a summation over 20 evenly spaced values of cosine from 0 to 1.

Fits to the progressive power saturation data in Figure 4 employing eq 20 and to the temperature dependence of the relaxation rates in Figure 6 employing a power law equation were found using Kaleidagraph (Abelbeck Software/Synergy Software), which also employs the Marquardt algorithm.

Sample temperatures were controlled by an Oxford ESR-900 cryostat system. Sample temperatures were measured using a gold-chromel thermocouple held in a sample tube at the same position.

Theory. We start by considering an enzyme with two spins deeply buried in the protein matrix and hence isolated from interenzyme magnetic interactions. In our model system this isolated pair of electron spins is in a static magnetic field, with a "slow" relaxing spin and a "fast" relaxing spin at a fixed distance r apart. The interspin vector $\mathbf{r}$ from the slow to the fast relaxing spin is in a random but fixed orientation with respect to the static magnetic field, and slow or fast relaxation is simply defined by the relative intrinsic relaxation rates of the two spins. Both spins are assumed to be isotropic. For the purpose of this discussion, the "observed spin" is the slow relaxing spin.

In the system described above, there are three contributions to the spin–lattice and transverse relaxation rates of the observed spin. The first is the intrinsic relaxation rate, k_{1i} (spin–lattice) or k_{2i} (transverse), which is defined as the relaxation rate of the observed spin in its native matrix in the absence of the fast relaxing spin.

A second contribution to the observed spin–lattice and transverse relaxation rates will arise from scalar exchange coupling if there is spatial overlap in the orbital wave functions of the unpaired spins. Abragam (1961) has solved the physically analogous problem for the scalar relaxation of a nuclear spin I by an electron spin S through their hyperfine coupling. His solution treats the fast relaxing spin S as a part of the lattice with the assumption that it is in thermal equilibrium because of its short relaxation time. Substituting the scalar exchange coupling, J_{ex}, for the hyperfine coupling, A, and changing the subscripts we can write

$$k_{1ex} = \frac{2(J_{ex})^2}{3} J(J+1) \frac{T_{2f}}{1+(\omega_s - \omega_f)^2 T_{2f}^2} \tag{3}$$

$$k_{2ex} = \frac{(J_{ex})^2}{3} J(J+1) \left[\frac{T_{2f}}{1+(\omega_s - \omega_f)^2 T_{2f}^2} + T_{1f} \right] \tag{4}$$

where T_{1f} and T_{2f} are the spin–lattice and transverse relaxation times of the fast relaxing spin, ω_s and ω_f are the Larmour frequencies of the observed (slow) and fast spins, respectively, and J is the spin quantum number of the fast relaxing spin.

The third contribution to the observed relaxation rates comes from the dipolar interaction between the two paramagnetic sites. Following the methods outlined by Abragam (1961), the appropriate equations have been derived by Kulikov and Likhtenstein (1977) and by Goodman and Leigh (1985).

$$k_{1\theta} = \frac{1}{T_{1\theta}} = \frac{\gamma_s^2 \mu_f^2}{r^6} \left(\frac{1}{6}B + 3C + \frac{3}{2}E \right) \tag{5}$$

$$k_{2\theta} = \frac{1}{T_{2\theta}} = \frac{\gamma_s^2 \mu_f^2}{r^6} \left(\frac{1}{3}A + \frac{1}{12}B + \frac{3}{2}C + 3D + \frac{3}{4}E \right) \tag{6}$$

where γ_s is the magnetogyric ratio for the slow spin, μ_f is the

magnetic dipole moment of the fast relaxing spin, r is the interspin distance, and θ is the angle between the magnetic field and the interspin vector. The terms A–E are defined as follows:

$$A = T_{1f}(1 - 3\cos^2\theta)^2 \quad (7)$$

$$B = \frac{T_{2f}}{1 + (\omega_s - \omega_f)^2 T_{2f}^2}(1 - 3\cos^2\theta)^2 \quad (8)$$

$$C = \frac{T_{1f}}{1 + \omega_s^2 T_{1f}^2}\sin^2\theta\cos^2\theta \quad (9)$$

$$D = \frac{T_{2f}}{1 + \omega_f^2 T_{2f}^2}\sin^2\theta\cos^2\theta \quad (10)$$

$$E = \frac{T_{2f}}{1 + (\omega_s + \omega_f)^2 T_{2f}^2}\sin^4\theta \quad (11)$$

Equations 3–6 are valid within the Redfield limit. For eqs 3 and 5 this limit requires that T_{1f} and $T_{2f} \ll T_{1s}$; for eqs 4 and 6 the Redfield limit requires that T_{1f} and $T_{2f} \ll T_{2s}$.

To summarize, the observed rates of spin–lattice and spin–spin relaxation can be described by

$$k_{1obs}(\theta) = k_{1scalar} + k_{1\theta} \quad (12)$$

$$k_{2obs}(\theta) = k_{2scalar} + k_{2\theta} \quad (13)$$

where the scalar rate constant in eq 12 represents the sum of the isotropic contributions, k_{1i} and k_{1ex}, and the scalar rate constant in eq 13 represents the sum of the isotropic contributions, k_{2i} and k_{2ex}. For any one orientation of the interspin vector, the saturation–recovery transient will be described by a single exponential, $k_{1obs}(\theta)$. However, since the relaxation rate is a function of θ and our actual sample has a random distribution of orientations, the observed saturation–recovery transient will be the sum of many different exponential recoveries, i.e.,

$$I(t) = 1 - N\int_0^{\pi} \sin\theta[e^{-(k_{1scalar} + k_{1\theta})t}]\, d\theta \quad (14)$$

where $I(t)$ is the intensity of the saturation–recovery transient at time t and N is an adjustable scaling factor. A similar equation has been proposed by Hyde et al. (1979).

An additional assumption in the analysis of the saturation–recovery transient should be discussed. Limitations on the power and the length of our saturating pulse allow us to "saturate" only a fraction of the total line width of an EPR absorption signal. In effect one can only observe those spin packets which contribute to the signal at the chosen resonant field position. Consider the case where the broadening of the observed absorption signal due to an anisotropic interaction is large compared to other sources of inhomogeneous broadening. Since the interspin vector is fixed relative to the anisotropic g or hyperfine tensor, choosing a particular field position within the absorption signal corresponds to restricting the accessible values of θ in eq 14 above. In the case of $Y_D^{\bullet}$, the anisotropic contribution to the hyperfine tensor is much less than the isotropic contribution (Barry & Babcock, 1988), and we make the approximation that by choosing the center of the EPR signal we get a statistical contribution from all orientations of the interspin vector to the saturation–recovery transient.

Equation 14 is completely general for the two-spin model we have described. Explicit evaluation of eq 14 requires knowledge of T_{1f}, T_{2f}, ω_s, ω_f, and r. There are two limits in which the expression for the dipolar contribution to the spin–lattice relaxation rate is particularly simple and in which knowledge of either T_{1f} or T_{2f} is unnecessary. For a very fast relaxing spin, i.e.,

$$(\omega_s + \omega_f)^2 T_{2f}^2,\ \omega_s{}^2 T_{1f}^2,\ (\omega_s - \omega_f)^2 T_{2f}^2 \ll 1$$

eq 5 becomes

$$k_{1\theta} = \frac{\gamma_s^2\mu_f^2}{r^6}\left[\frac{1}{6}T_{2f}(1 - 3\cos^2\theta)^2 + 3T_{1f}\sin^2\theta\cos^2\theta + \frac{3}{2}T_{2f}\sin^4\theta\right] \quad (15)$$

If $T_{1f} \gg T_{2f}$, the "C" term will dominate and T_{2f} can be ignored. For eq 15 to apply at X-band (ν = 9.0 GHz) for two spins near g = 2.0 requires that T_{1f} and $T_{2f} \ll 10^{-11}$ s.

In the opposite limit where

$$\omega_f^2 T_{1f}^2,\ (\omega_s + \omega_f)^2 T_{2f}^2, \text{ and } (\omega_s - \omega_f)^2 T_{2f}^2 \gg 1$$

eq 5 becomes

$$k_{1\theta} = \frac{\gamma_s^2\mu_f^2}{r^6}\left[\frac{(1 - 3\cos^2\theta)^2}{6(\omega_s - \omega_f)^2 T_{2f}} + \frac{3\sin^2\theta\cos^2\theta}{\omega_s^2 T_{1f}} + \frac{3\sin^4\theta}{2(\omega_s + \omega_f)^2 T_{2f}}\right] \quad (16)$$

For eq 16 to apply at X-band requires that T_{1f} and $T_{2f} \gg 10^{-11}$ s, reasonable limits for a first row transition metal near or below liquid-nitrogen temperatures.

If in addition $(\omega_s - \omega_f)^2 \ll \omega_s^2$ and $(\omega_s + \omega_f)^2$, the "B" term will dominate $k_{1\theta}$ in eq 16. For EPR, the resonance condition is more naturally described by the g value of the paramagnetic species. By factoring out ω_s from the inequality above and using the relation $\omega = g\beta H 2\pi/h$, one can restate the inequality as $(1 - g_f/g_s)^2 \ll 1$ and $(1 + g_f/g_s)^2$, where g_s and g_f are the g values of the fast and slow relaxing spins, respectively. If this inequality holds true, i.e., the "B" term dominates the dipolar relaxation, we can rewrite eq 16 in terms of a dipolar rate constant k_{1d}:

$$k_{1\theta} = k_{1d}(1 - 3\cos^2\theta)^2 \quad (17)$$

where

$$k_{1d} = \frac{\gamma_s^2\mu_f^2}{6r^6\omega_s^2(1 - g_f/g_s)^2 T_{2f}} \quad (18)$$

Evaluation of a saturation–recovery transient using eqs 14 and 17 will yield two rate constants, $k_{1scalar}$ and k_{1d}. If γ_s, μ_f, g_s, g_f, and T_{2f} are known, the distance r can be determined from k_{1d} using eq 18. In addition, the presence of scalar exchange coupling can be inferred if the scalar rate constant is significantly greater then the intrinsic relaxation rate k_{1i}. In the same limit for T_{2f}, i.e., $T_{2f} \gg 10^{-11}$ s, eq 3 becomes

$$k_{1ex} = \frac{2(J_{ex})^2}{3}\frac{J(J + 1)}{\omega_s^2(1 - g_f/g_s)^2 T_{2f}} \quad (19)$$

In this case, knowledge of J, g_s, g_f, and T_{2f} allows evaluation of the exchange coupling J_{ex} in eq 19. Finally, we note that equations analogous to 14, 17, 18, and 19 can be derived for the phase-memory or "T_2" experiment.

Results and Discussion

Anomalous Spin–Lattice Relaxation of $Y_D^{\bullet}$. We find that in Mn-depleted PSII, signal II$_s$ ($Y_D^{\bullet}$) relaxes with nonexponential kinetics over the 5–70 K temperature range, while the

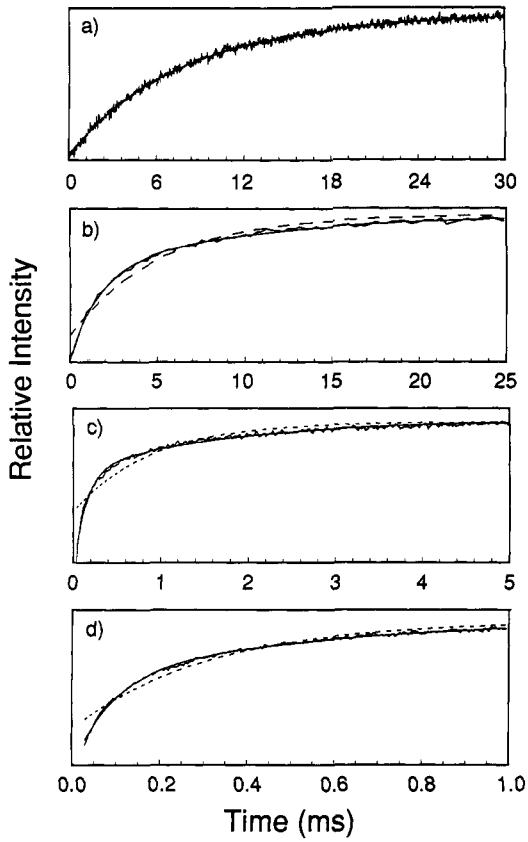

FIGURE 2: Saturation–recovery transients observed at 20 K for (a) the UV-generated model L-tyrosine radical, and the stable tyrosine radical $Y_D^\bullet$ in (b) Mn-depleted PSII membranes, (c) S_1-state PSII membranes, and (d) S_2-state PSII membranes. Single-exponential (dashed line) and double-exponential (solid line) fits are shown superimposed upon the experimental traces. The traces are arbitrarily scaled vertically; note the different time scales for each case. The observing microwave power level was 1.80 μW.

L-tyrosine radical exhibits single-exponential spin–lattice relaxation kinetics at these temperatures. Our analysis of the anomalous relaxation behavior of $Y_D^\bullet$ is based on the assumption that a dipolar interaction between $Y_D^\bullet$ and the non-heme Fe(II) produces a powder-pattern distribution of spin–lattice relaxation rates. However, there are other plausible explanations which we will examine first. It has been proposed that the nonexponential relaxation behavior of $Y_D^\bullet$ is the result of redox heterogeneity in PSII (Evelo et al., 1989). We also consider the possibility that the EPR signal associated with $Y_D^\bullet$(signal II_s) arises from more than one radical species or that the anomalous relaxation behavior of $Y_D^\bullet$ is the result of a dipolar interaction with a paramagnetic site other than the non-heme Fe(II).

We consider first the possibility that redox heterogeneity of the Mn center in PSII causes the nonexponential spin–lattice relaxation of $Y_D^\bullet$. In their first paper describing spin-echo detected T_1 measurements of $Y_D^\bullet$, Evelo et al. (1989) accounted for the nonexponential relaxation properties of $Y_D^\bullet$ in terms of a weak dipolar interaction between it and the Mn complex in the OEC. The relaxation kinetics of $Y_D^\bullet$ were modeled with a rate law incorporating two exponential rate constants, which were assigned to two distinct Mn–$Y_D^\bullet$ distances arising from cryogenic trapping of valence states in the Mn complex. Figure 2 presents examples of the spin–lattice relaxation transients observed at 22 K with $Y_D^\bullet$ in native (S_1 state and S_2 state) and Mn-depleted PSII membranes in comparison with relaxation transients observed with the model L-tyrosine radical. $Y_D^\bullet$ relaxes with kinetics that are more

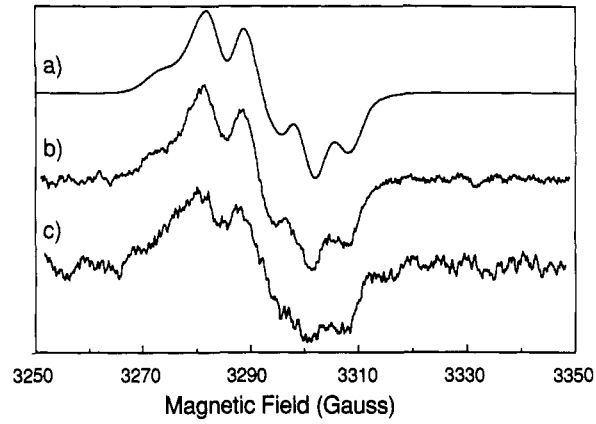

FIGURE 3: Time-resolved, field-swept, first-derivative EPR spectra of $Y_D^\bullet$ in S_2-state PSII obtained at 22 K by boxcar averaging at fixed delays following at 200-μs saturating microwave pulse. A conventional continuous-wave EPR spectrum, obtained as described in Figure 1, is shown in spectrum a for comparison to the time-resolved spectra obtained at (b) 40 μs and (c) 300 μs during the recovery from saturation. In spectra b and c the derivative was calculated from the absorption mode spectra actually acquired; the gate of the boxcar averager was 10 μs wide, the microwave frequency was 9.04 GHz, and the saturating pulse repetition rate was 145 Hz.

adequately described by a rate law incorporating two evenly weighted exponential relaxation components than by a single exponential relaxation component (Figure 2b–d). However, while the relaxation of $Y_D^\bullet$ occurs more rapidly in the presence of a functional S_1-state or S_2-state Mn complex (Figure 2c,d), nonexponential relaxation traces are observed from $Y_D^\bullet$ even in the absence of the Mn complex (Figure 2b). The deviation from a single exponential is just as great in the Mn-depleted sample as in the samples having a functional Mn complex present. The model L-tyrosine radical, however, exhibits single-exponential relaxation traces (Figure 2a). The fact that even Mn-depleted PSII shows nonexponential recovery does not by itself disprove the original hypothesis of Evelo et al. (1989). However, a simpler explanation is that, in both Mn-depleted and in Mn-containing PSII, a dipolar interaction and the random distribution of orientations produces a powder distribution of relaxation rates.

The presence of a chemically distinct radical species at the same resonant field position could produce a biexponential recovery for signal II_s. However, Figure 3 shows that the relaxation transients exhibited by $Y_D^\bullet$ arise from a single chemical entity. A boxcar averager was employed to record a time-resolved, field-swept EPR spectrum from $Y_D^\bullet$ in S_2-state PSII membranes at two delay settings following the saturating microwave pulse that began the saturation–recovery experiment. Similar spectra were obtained with S_1-state PSII membranes although lower signal/noise ratios were obtained. The faster relaxation of $Y_D^\bullet$ in the S_2 state allowed higher pulse repetition frequencies and better averaging of signals. The line shape exhibited by $Y_D^\bullet$ at 40 and 300 μs following the microwave pulse (Figure 3b,c) is the same as that recorded by a conventional continuous EPR experiment (Figure 3a). Hence, it is unlikely that two or more radical species contribute to the observed relaxation transient. It is also improbable that another radical entity interferes with the measurement, since a semiquinone or chlorophyll radical would exhibit a much different EPR line shape. Thus, the explanation that the two observed exponential relaxation rate constants arise from two distinct radical species in PSII can be rejected. The nonexponential relaxation properties of $Y_D^\bullet$ must arise, then, from interactions of $Y_D^\bullet$ with neighboring relaxers in all PSII centers.

We have considered the possibility that a paramagnetic species other than Fe(II) is involved in the dipole–dipole induced relaxation of $Y_D^{\bullet}$. There are several paramagnetic sites in the PSII reaction center, in addition to the Mn complex, that might act as relaxation rate enhancers for $Y_D^{\bullet}$. Radical species, such as the other tyrosine radical in PSII, $Y_Z^{\bullet}$, or the cryogenically trapped chlorophyll cation radical that is formed under illumination at temperatures below 120 K in functional PSII membranes (de Paula et al., 1985, 1986), relax too slowly to provide an efficient relaxation enhancement for $Y_D^{\bullet}$. Cytochrome b_{559} is unlikely to enhance the relaxation of $Y_D^{\bullet}$. It is apparently far enough away that direct electron transfer to $Y_D^{\bullet}$ is not observed, and, being low spin, cytochrome b_{559} is expected to be a relatively weak relaxation rate enhancer. In addition to the non-heme Fe(II) and the low-spin Fe(II)/(III) of cytochrome b_{559}, the $g = 4.3$ "turning point" of rhombic iron was always present in our samples. Since the hydroxylamine treatment used to remove the manganese from the OEC also includes washes with EDTA, it is unlikely that the relaxation enhancement observed is due to adventitious binding of iron or other paramagnetic ions. While the possibility that there is a structural/functional Fe(II)/(III) bound near Y_D cannot be excluded at this time, we found that while the intensity of the $g = 4.3$ turning point varied from preparation to preparation relative to that of cytochrome b_{559} or $Y_D^{\bullet}$, the saturation–recovery relaxation kinetics were unaffected.

On the other hand, it is fairly certain that the non-heme Fe(II) in PSII is bound by the same D2 polypeptide that contains the tyrosine which functions as Y_D. The histidine ligands to the non-heme Fe(II) in the M subunit of the bacterial reaction center are conserved in the D2 polypeptide of PSII (Michel & Deisenhofer, 1988). This high-spin Fe(II) species is expected to be an excellent electron spin relaxation enhancer for $Y_D^{\bullet}$. In the photosynthetic reaction center in purple non-sulfur bacteria, the analogous non-heme Fe(II) site enhances the relaxation of the radical cation of the "special pair" reaction center chlorophyll (Norris et al., 1980).

Anomalous Progressive Power Saturation Behavior of $Y_D^{\bullet}$. Beinert and Orme-Johnson (1967) have shown that in the limit of an inhomogeneously broadened line, the effect of progressive power saturation can be described by

$$S = K\sqrt{P}/(1 + P/P_{1/2})^{1/2} \qquad (20)$$

where S is the EPR absorption signal amplitude, P is the applied microwave power, and $P_{1/2}$ is the microwave power at half-saturation. K is simply a scaling factor. We examined the progressive power saturation behavior of three tyrosine radicals at 7.0 K: $Y_D^{\bullet}$, the UV-generated L-tyrosine radical in a borate glass, and the tyrosine radical in the B2 subunit of ribonucleotide reductase. Our saturation–recovery measurements on the UV-generated tyrosine radical indicate that it behaves like an isolated spin. At 7.0 K the tyrosine radical of ribonucleotide reductase of *E. coli* is also expected to behave like an isolated spin; at this temperature the nearby antiferromagnetically coupled diferric center is in its $S = 0$ ground state (Sahlin et al., 1987).

The results of progressive power saturation for each radical are plotted as log $(S/\sqrt{P})$ vs log P in Figure 4. The signal amplitude, S, was measured as shown in Figure 1. Equation 20 predicts that a curve drawn through these points will be linear in two regions. In the limit that $P \ll P_{1/2}$, log $(S/\sqrt{P})$ remains constant. In the limit where $P \gg P_{1/2}$, log $(S/\sqrt{P})$ will exhibit a linear dependence on log P, with a slope $m = -1/2$. In the presence of dipole–dipole induced relaxation, eqs 12 and 13 predict that $P_{1/2}$ will be a function of the orientation

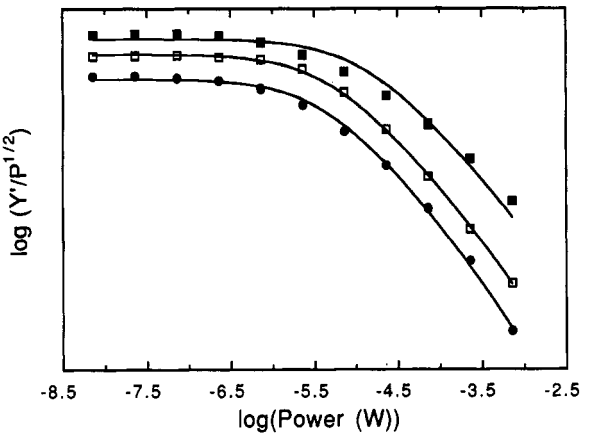

FIGURE 4: Continuous microwave power saturation of the EPR signals from (■) $Y_D^{\bullet}$ in Mn-depleted PSII, (□) the UV-generated L-tyrosine radical, and (●) the tyrosine radical in ribonucleotide reductase from *E. coli*. The solid lines are fits to eq 20. The vertical positions of the curves are offset arbitrarily. Conditions: temperature, 7.0 K; field modulation width, 2.0 G; field modulation frequency, 100 kHz; microwave frequency, 9.05 GHz. The peak-to-peak height (Y') was measured as illustrated in Figure 1.

of the interspin vector with respect to the static magnetic field. This will *not* effect the progressive power saturation behavior in the two limits just described. In other words, if $P \ll P_{1/2\text{min}}$, where $P_{1/2\text{min}}$ is the minimum value of $P_{1/2}$ in the sample, then log $(S/\sqrt{P})$ will be constant. If $P \gg P_{1/2\text{max}}$, then log $(S/\sqrt{P})$ will exhibit a linear dependence on log P with a slope $m = -1/2$. However, since there is a range of $P_{1/2}$ values, the "curved region" between these two limits will be longer and the radius of curvature will be greater.

The experimental results for each tyrosine radical were fit using eq 20 allowing K and $P_{1/2}$ values to vary simultaneously. These fits are shown superimposed on the data in Figure 4. Equation 20 fits the data well for both the UV-generated tyrosine radical and the tyrosine radical of ribonucleotide reductase, and the fitted $P_{1/2}$ values are approximately equal, 3.7 and 3.2 μW, respectively. In contrast, the data for $Y_D^{\bullet}$ are fit poorly by eq 20. In the transition from $P \ll P_{1/2}$ to $P \gg P_{1/2}$, i.e., at the higher power points in Figure 4, the radius of curvature is greater for $Y_D^{\bullet}$ than it is for either of the other two species. The fitted $P_{1/2}$ value for $Y_D^{\bullet}$ of 9.1 μW is significantly higher than for the other two radicals.

For line shapes which are neither perfectly inhomogeneous nor homogeneous, the absorption amplitude can be empirically fit to the function

$$S = K\sqrt{P}/(1 + P/P_{1/2})^{b/2} \qquad (21)$$

where b is the inhomogeneity parameter determined by the ratio of Lorentzian spin packet width to the Gaussian envelope width. For the EPR derivative amplitude, $b = 1.0$ and $b = 3.0$ represent the inhomogeneous and homogeneous limits, respectively. If we use this function to fit the data and now allow b to vary as well, we find that the UV-generated tyrosine radical and the tyrosine radical of ribonucleotide reductase give b values close to 1.0, i.e., 1.03 and 0.95, respectively, and that their fitted $P_{1/2}$ values are changed by less than 1.0 μW. On the other hand, the fit to the data from $Y_D^{\bullet}$ gives $b = 0.71$ and a $P_{1/2}$ of 2.4 μW. While a "b value" of 0.71 provides a better fit to the data for $Y_D^{\bullet}$, it is not a physically meaningful inhomogeneity parameter. The fact that the fitted b value for the tyrosine radical in ribonucleotide reductase is slightly less than 1 may indicate that there is a small dipolar contribution to the spin–lattice or phase memory relaxation due to the

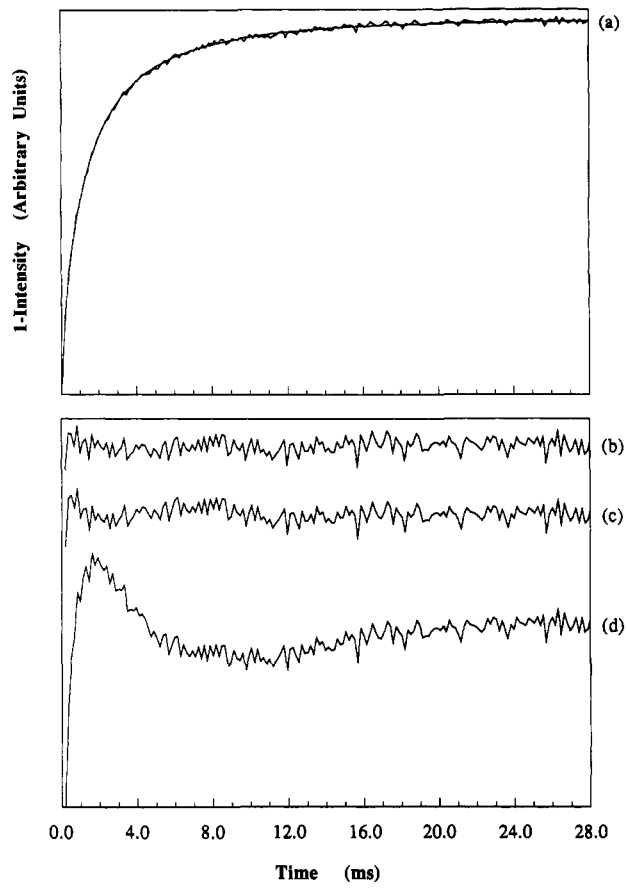

FIGURE 5: (a) Saturation–recovery transient obtained for $Y_D^\bullet$ in Mn-depleted PSII membranes at 25 K and the fit by the orientation-dependent rate law (eqs 14 and 17). The observing microwave level was 4.5 μW, and the saturating microwave pulse (230 mW) was of 10-ms duration. The residuals for fits to the observed transient by (b) the orientation-dependent rate law, (c) a double exponential, and (d) a single exponential are plotted using an expanded vertical scale.

neighboring diferric center, even an 7.0 K.

Application of the Model Equations. The rate constant k_{1i} can be measured experimentally in one of two ways. The first is to remove the fast relaxing spin from the protein, either directly or by oxidation/reduction. The second is to model the intrinsic relaxation rate of the observed spin using a chemically identical species in an environment free of the fast relaxing spin. We chose the latter course, using photochemically generated and cryogenically trapped L-tyrosine radicals in a borate glass to model the intrinsic relaxation of $Y_D^\bullet$. This model system was exploited previously by Sahlin et al. (1987) in their study of the continuous power saturation and EPR line shape properties of the tyrosyl radical in ribonucleotide reductase. Their study suggests that the relaxation behavior of the model L-tyrosine radical exemplifies the behavior of a tyrosine radical within a protein matrix in the absence of perturbations from neighboring paramagnetic ions. At temperatures below 30 K, the relaxation rate product, $(T_1T_2)^{-1}$, for the tyrosine radical in ribonucleotide reductase from *E. coli* and the L-tyrosine radical are equal within experimental error (Sahlin et al., 1987). In addition, T_1 measurements performed earlier on ribonucleotide reductase (Beck et al., 1991) and those quoted here on the L-tyrosine radical indicate that these values are also equal within experimental error.

Saturation–recovery transients were collected as described in the under Materials and Methods over a temperature range of 5–70 K. Figure 5a, shows a saturation–recovery trace from $Y_D^\bullet$ in Mn-depleted PSII and the best fit of the dipolar model.

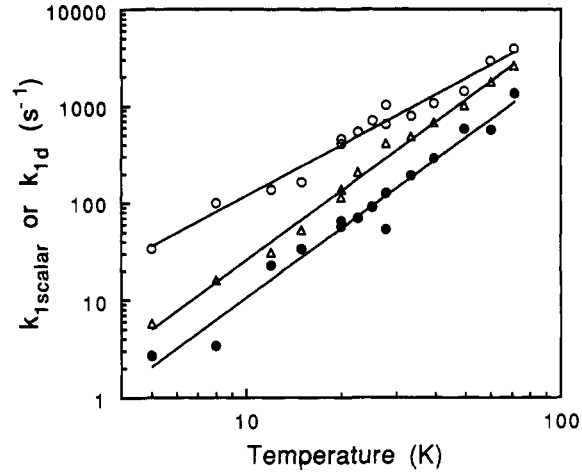

FIGURE 6: Scalar and orientation-dependent electron-spin relaxation rate constants [$k_{1scalar}$ (●) and k_{1d} (○), respectively] for $Y_D^\bullet$ obtained as a function of sample temperature in Mn-depleted PSII membranes. $k_{1scalar}$ and k_{1d} were obtained by fitting the orientation-dependent rate law, eqs 14 and 17, to saturation–recovery transients at each temperature. The single-exponential electron spin–lattice relaxation rates for the UV-generated model tyrosine radical (△) are plotted in order to allow comparison with the $k_{1scalar}$ constants of $Y_D^\bullet$. The equations $k_{1scalar} = 0.0459 \times T^{2.36}$ and $k_{1d} = 2.21 \times T^{1.73}$ have been fit to the temperature-dependent relaxation rates of $Y_D^\bullet$. The equation $k_{1scalar} = 0.111 \times T^{2.37}$ has been fit to the temperature-dependent relaxation of the L-tyrosine radical.

As demonstrated by the residual traces presented in Figure 5b,c, eq 14 fits the relaxation transient as well as the two-exponential model and does so with one less adjustable parameter. Figure 5d demonstrates that the recovery is poorly fit by a single exponential.

Figure 6 presents the rate constants $k_{1scalar}$ and k_{1d} for $Y_D^\bullet$ and a single-exponential fit for the UV-generated tyrosine radical, in which case $1/T_1$ is treated as $k_{1scalar}$. The scalar relaxation rate of $Y_D^\bullet$ is slightly less than the spin–lattice relaxation rate of the L-tyrosine radical, probably resulting from differences in the local environment of the two radicals. Note that a contribution of scalar exchange to $k_{1scalar}$ of $Y_D^\bullet$ would be expected to result in $k_{1scalar}$ of $Y_D^\bullet$ being *larger* than the spin–lattice relaxation rate of the L-tyrosine radical. In addition, the temperature dependence of $1/T_1$ of the L-tyrosine radical and $k_{1scalar}$ of $Y_D^\bullet$ are both proportional to $T^{2.4}$. Equations 18 and 19 indicate that if scalar exchange were the primary contribution to the scalar rate constant, then $k_{1scalar}$ and k_{1d} would have the same (or nearly the same) temperature dependence. However, as shown in Figure 6, the temperature dependence of k_{1d} is proportional to $T^{1.7}$ in this temperature range. These results indicate that the primary contribution to $k_{1scalar}$ of $Y_D^\bullet$ is the intrinsic relaxation, k_{1i}, of the radical.

The dipolar interaction between the non-heme Fe site and $Y_D^\bullet$ leads to a temperature-dependent electron spin–lattice relaxation enhancement (Figure 6). The temperature dependence of k_{1d} indicates that eqs 16 and 17 represent the correct limit for evaluation of $k_{1\theta}$. In eq 17, k_{1d} is proportional to $1/T_{2f}$, indicating that k_{1d} (and hence $k_{1\theta}$) should remain constant or increase with temperature. In the opposite limit, eq 15 with the "*C*" term dominant, k_{1d} would be directly proportional to T_{1f}, indicating that k_{1d} should *decrease* with increasing temperature. The significant temperature dependence of T_{2f} is perhaps surprising. The conventional wisdom in continuous wave microwave power-saturation experiments has been that T_{2f} is independent of temperature in the temperature range we have explored. Apparently for high-spin Fe(II), either T_{2f} is limited by T_{1f} because of rapid spin–lattice relaxation or T_{2f} has its own temperature dependence due to

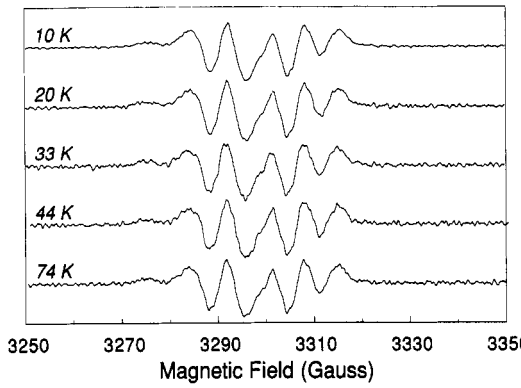

FIGURE 7: Second-derivative, continuous-wave EPR spectra of $Y_D^\bullet$ obtained as a function of temperature in S_1-state PSII membranes. The second derivative was calculated from the digitized first-derivative spectra; the field-modulation amplitude was 0.4 G, and the observing microwave power level was 5 μW; otherwise conditions were as in Figure 1.

couplings between lattice vibrations and the crystal field of the iron.

The dipolar interaction responsible for the enhancement of the spin–lattice relaxation might be expected to shorten the phase-memory time (T_{2s}) of $Y_D^\bullet$ and produce a powder distribution of rates. One could investigate this directly by doing a spin-echo experiment. On the other hand, a significant shortening of T_{2s} should manifest itself in a cw experiment as the "Leigh effect" (Leigh, 1970), i.e., an apparent decrease in the absorption signal intensity or an increase in the signal line width with *decreasing* temperature as a result of dipolar interactions between a pair of paramagnetic centers. However, we find (data not shown) that in Mn-depleted PSII, the intensity of the EPR signal from $Y_D^\bullet$ shows Curie Law behavior from 7 to 71 K. Even in oxygen-evolving PSII membranes where the relaxation enhancement of $Y_D^\bullet$ is much greater, we see Curie Law behavior from 13 to 220 K (Innes & Brudvig, 1989). Leigh (1970) predicted in his original paper that outside the Redfield limit of $T_{1f} \ll T_{2s}$, one would expect the broadened peak to split into two peaks which would finally resolve into a Pake doublet when $T_{1f} \gg T_{2s}$. We find, however, that the EPR line shape exhibited by $Y_D^\bullet$ is essentially constant from 10 to 74 K, as is apparent from the series of higher resolution, second-derivative spectra shown in Figure 7 that were recorded with a S_1-state PSII membrane sample. We cannot rule out the existence of T_2 relaxation enhancement of $Y_D^\bullet$ on the basis of these experiments, particularly at temperatures below 7 K. However, these experiments place a limit on the magnitude of this relaxation enhancement. Note that the EPR line shape exhibited by the tyrosyl radical in ribonucleotide reductase, in contrast, exhibits a significant broadening as the temperature is *increased* owing to increasingly strong perturbations from the adjacent diferric site (Sahlin et al., 1987).

Calculating a Y_D–Fe(II) Distance. If eq 17 applies and γ_s, μ_f, g_s, g_f, and T_{2f} are known, the distance r can be determined from k_{1d} using eq 18. Since the magnetic properties of the non-heme iron in PSII have not been experimentally determined, we must rely on measurements on the high-spin non-heme Fe(II) in reaction centers from *Rb. sphaeroides*. There is reason to believe that the magnetic properties of the two iron centers are very similar. In the bacterial reaction centers the non-heme Fe(II) has four histidine and one bidentate carboxylate ligands. Sequence homologies in PSII (Michel & Deisenhofer, 1988) indicated that its high-spin iron has the same ligand set with the exception that the carboxylate may be replaced with a bicarbonate anion (Eaton-Rye & Govindjee, 1988; Diner & Petrouleas, 1990). The non-heme Fe(II) in *Rb. sphaeroides* has been well characterized by Butler et al. (1980) using static magnetic measurements on Fe(II) and EPR measurements (Butler et al., 1984) on the weakly exchange-coupled Fe(II)–quinone radical anion system. Their measurements indicate that, for Fe(II), $g_{av} = 2.17$. This is a good approximation to g_{av} of Fe(II) in PSII because the Fe(II)–Q_A^- EPR signals in PSII and bacterial reaction centers are quite similar (Nugent et al., 1981; Rutherford & Zimmermann, 1984). The g value of $Y_D^\bullet$ is known to be 2.00. The "*B*" term dominates since $g_f = g_{av}[\text{Fe(II)}] = 2.17$, and $g_s = g(Y_D^\bullet) = 2.00$, and hence $(1 - g_f/g_s)^2 \ll 1$ and $(1 + g_f/g_s)^2$. Therefore, we can use eq 18 to estimate the distance between the tyrosine radical, $Y_D^\bullet$, and the non-heme Fe(II). We take $\gamma_s = \gamma_e$, $\mu_f = \mu^{Fe(II)} = 5.35\ \beta$ (Butler et al., 1980), and $\omega_s = 9.05$ GHz. Substituting into eq 18 and rearranging the terms, we find that

$$r^6 = \frac{5.43 \times 10^{-45}\ \text{cm}^6}{k_{1d} T_{2f}} \qquad (22)$$

Values of k_{1d} are available from our experiments over the temperature range 5–77 K. If T_{2f} is known somewhere in this temperature range, we can calculate the distance using eq 22. While no direct observation of T_{2f} has been made in either PSII or bacterial reaction centers, Calvo et al. (1982) have studied the low-temperature (<4 K) spin–lattice relaxation behavior of the Fe(II)–semiquinone species in reaction centers from *Rb. sphaeroides*. They show that the temperature dependence of the spin–lattice relaxation rate is well fit by an equation which assumes that relaxation is a two-step process in analogy with the Orbach process. Using their equation and the dominant component of the exchange interaction between the Fe(II) and semiquinone, $J_y = 0.58$ K (Butler et al., 1984), one can estimate T_1 of the non-heme iron itself. We estimate T_1 of the iron to be 5.6×10^{-8} s at 5 K. Using this value of T_{1f} and our measured value for k_{1d} of 34 s^{-1} at 5 K in eq 22, we calculate an Fe(II)–$Y_D^\bullet$ distance of 38 Å. Since $T_{2f} \leq T_{1f}$, this sets an upper limit on T_{2f} and a lower limit on the Fe(II)–$Y_D^\bullet$ distance. This is in good agreement with the prediction of 36.8 Å based on the assumption of structural similarities between reaction centers from *Rps. viridis* and PSII.

Conclusion

We show that, in cases where a dipolar interaction with a neighboring spin mediates electron spin–lattice relaxation, theory predicts that a powder distribution of relaxation rates will be observed in a rigid sample. Thus, the distinctive non-exponential relaxation traces observed from $Y_D^\bullet$ in Mn-depleted PSII membranes can be explained in terms of a dipolar interaction with the non-heme Fe(II). The magnitude of the dipolar relaxation rate constant can then be used to determine the distance between the two spins, if the g values and T_{2f} are known. We have used saturation–recovery EPR to obtain the magnitude of the dipolar interaction between $Y_D^\bullet$ and the high-spin non-heme Fe(II) in Mn-depleted PSII and have used this value to calculate the distance between them. While applying the derived equations to a situation where the relaxing spin is an $S = 2$ center ignores several complicating factors that arise when $S > 1/2$, we note that this relatively simple analysis provides an overall picture which is both qualitatively and quantitatively reasonable.

Use of our approach should also allow the assessment of electron transfer probabilities via measurement of the scalar exchange enhancement of spin–lattice relaxation. The same electronic matrix element is found in the expression for k_{1ex},

the scalar exchange rate constant, and the rate constant for long-range electron transfer (Goodman & Leigh, 1985). Therefore measurements of electron spin relaxation may afford a powerful indirect probe of electron transfer in multisite redox enzymes. In the case of $Y_D^{\bullet}$, its fast relaxing partner apparently causes little or no enhancement of spin–lattice relaxation by scalar exchange. This is not surprising for the non-heme iron, since there is no evidence of direct electron transfer between these two sites.

A progressive power saturation experiment can also indicate the presence of a dipolar interaction. In the presence of a dipolar interaction, one expects that the experimental points, plotted as log $(S/\sqrt{P})$ vs log P, will be poorly fit by eq 20 in the "curved region" between the two linear limits and that the fitted $P_{1/2}$ value will be greater than that for an isolated spin. This was observed for $Y_D^{\bullet}$. However, the value of $P_{1/2}$ alone does not reflect the relative contributions of dipolar, scalar exchange, or "intrinsic" relaxation processes. In principle, the dipolar contribution to the relaxation rate could be extracted from a $P_{1/2}$ experiment by explicitly including the orientation dependence of T_{1s} and T_{2s} in the fit. However, doing so would require at least two additional fitting parameters (if $T_{1f} \neq T_{2f}$), and it is not clear that meaningful scalar and dipolar contributions to $P_{1/2}$ could be extracted.

The approach outlined in this paper for the analysis of electron spin–lattice relaxation transients is of general applicability. Future work will apply the approach described in this paper to several systems in which long-range electron transfer occurs. We have applied the method used in this paper to an analysis of the magnetic interaction between the tyrosyl radical and the Fe(III) dimer in ribonucleotide reductase. The results of that investigation will be published separately. An appropriate model system for the Fe(II)–$Y_D^{\bullet}$ interaction can be found in reaction centers from *Rb. sphaeroides*. A dipolar interaction has been observed between the radical P^+ and the non-heme Fe(II) in these reaction centers (Norris et al., 1980), and the distance between these two sites is already known from their crystal structures. We have started an investigation into the relaxation behavior of P^+ in bacterial reaction centers. Also, it is known that $Y_D^{\bullet}$ participates in the dark one-electron oxidation of the tetranuclear Mn coordination complex that serves as the H_2O oxidation catalyst in PSII. In the dark, $Y_D^{\bullet}$ is reduced and the Mn complex is oxidized from its S_0 oxidation state to the normally dark-stable S_1 state (Styring & Rutherford, 1987). This behavior suggests that the Mn complex and $Y_D^{\bullet}$ are near enough to each other to allow electron transfer between the two sites, suggesting that a scalar exchange interaction should be observable.

ACKNOWLEDGMENTS

Special thanks to John B. Lynch and Larry Que, Jr., for the ribonucleotide reductase sample used in this investigation. W.F.B. acknowledges support during preparation of the manuscript from the Miller Institute for Basic Research in Science in the form of a postdoctoral fellowship.

REFERENCES

Abragam, A. (1961) *The Principles of Nuclear Magnetism*, Chapter 8, Clarendon Press, Oxford.

Babcock, G. T., Barry, B. A., Debus, R. J., Hoganson, C. W., Atamian, M., McIntosh, L., Sithole, I., & Yocum, C. F. (1989) *Biochemistry 28*, 9557–9565.

Barry, B. A., & Babcock, G. T. (1988) *Chem. Scr. 28A*, 117–122.

Beck, W. F., de Paula, J. C., & Brudvig, G. W. (1985) *Biochemistry 24*, 3035–3043.

Beck, W. F., Innes, J. B., & Brudvig, G. W. (1990) *Current Research in Photosynthesis* (Baltscheffsky, M., Ed.) I.3, 817–820, Kluwer Academic Publishers, Dordrecht, The Netherlands.

Beck, W. F., Innes, J. B., Lynch, J. B., & Brudvig, G. W. (1991) *J. Magn. Reson. 91*, 12–29.

Beinert, H., & Orme-Johnson, W. H. (1967) in *Magnetic Resonance in Biological Systems* (Ehrenberg, A., Malmström, B. G., & Vänngård, T., Eds.) pp 221–247, Pergamon Press, Oxford.

Berthold, D. A., Babcock, G. T., & Yocum, C. F. (1981) *FEBS Lett. 134*, 231–234.

Britt, R. D., Sauer, K., & Klein, M. P. (1987) in *Progress in Photosynthesis Research* (Biggins, J., Ed.) I.5, 573–576, Martinus Nijhoff, Dordrecht, The Netherlands.

Butler, W. F., Johnston, D. C., Shore, H. B., Fredkin, D. R., Okamura, M. Y., & Feher, G. (1980) *Biophys. J. 32*, 967–992.

Butler, W. F., Calvo, R., Fredkin, D. R., Isaacson, R. A., Okamura, M. Y., & Feher, G. (1984) *Biophys. J. 45*, 947–973.

Calvo, R., Butler, W. F., Isaacson, R. A., Okamura, M. Y., Fredkin, D. R., & Feher, G. (1982) *Biophys. J. 37*, 111a.

de Groot, A., Plijter, J. J., Evelo, R., Babcock, G. T., & Hoff, A. J. (1986) *Biochim. Biophys. Acta 848*, 8–15.

de Paula, J. C., Innes, J. B., & Brudvig, G. W. (1985) *Biochemistry 24*, 8114–8120.

de Paula, J. C., Li, P. M., Miller, A.-F., Wu, B. W., & Brudvig, G. W. (1986) *Biochemistry 25*, 6487–6494.

Debus, R. J., Barry, B. A., Babcock, G. T., & McIntosh, L. (1988) *Proc. Natl. Acad. Sci. U.S.A. 85*, 427–430.

Diner, B. A., & Petrouleas, V. (1990) *Biochim. Biophys. Acta 1015*, 131–140.

Eaton-Rye, J. J., & Govindjee (1988) *Biochim. Biophys. Acta 935*, 248–257.

Evelo, R. G. (1990) Ph.D. Thesis, pp 99–116, State University of Leyden, Leyden, The Netherlands.

Evelo, R. G., Styring, S., Rutherford, A. W., & Hoff, A. J. (1989) *Biochim. Biophys. Acta 973*, 428–442.

Goodman, G., & Leigh, J. S., Jr. (1985) *Biochemistry 24*, 2310–2317.

Hales, B. J., & Das Gupta, A. (1981) *Biochim. Biophys. Acta 637*, 303–311.

Hyde, J. S. (1979) in *Time Domain Electron Spin Resonance* (Kevan, L., & Schwartz, R. N., Eds.) pp 1–30, John Wiley & Sons, New York.

Hyde, J. S., Swartz, H. M., & Antholine, W. E. (1979) in *Spin Labeling II: Theory and Applications* (Berliner, L. J., Ed.) pp 71–113, Academic Press, New York.

Innes, J. B., & Brudvig, G. W. (1989) *Biochemistry 28*, 1116–1125.

Isogai, Y., Nishimura, M., Iwaki, M., & Itoh, S. (1988) *Biochim. Biophys. Acta 936*, 259–268.

Kulikov, A. V., & Likhtenstein, G. I. (1977) *Adv. Mol. Relax. Interact. Processes 10*, 47–79.

Leigh, J. S., Jr. (1970) *J. Chem. Phys. 52*, 2608–2612.

Michel, H., & Deisenhofer, J. (1988) *Biochemistry 27*, 1–7.

Nishi, N. N., Hoff, A. J., Schmidt, J., & Van der Waals, J. H. (1978) *Chem. Phys. Lett. 58*, 164–170.

Norris, J. R., Thurnauer, M. C., & Bowman, M. K. (1980) *Adv. Biol. Med. Phys. 17*, 365–416.

Nugent, J. H. A., Diner, B. A., & Evans, M. C. W. (1981) *FEBS Lett. 124*, 241–244.

Press, W. H., Flannery, B. P., Teukolsky, S. A., & Vetterling, W. T. (1989) *Numerical Recipes in Pascal*, pp 574–580,

Cambridge University Press, Cambridge.
Rutherford, A. W., & Zimmermann, J.-L. (1984) *Biochim. Biophys. Acta 767*, 168-175.
Sahlin, M., Petersson, L., Gräslund, A., Ehrenberg, A., Sjöberg, B.-M., & Thelander, L. (1987) *Biochemistry 26*, 5541-5548.
Scholes, C. P., Janakiraman, R., Taylor, H., & King, T. E. (1984) *Biophys. J. 45*, 1027-1030.
Styring, S., & Rutherford, A. W. (1987) *Biochemistry 26*, 2401-2405.
Styring, S., & Rutherford, A. W. (1988) *Biochemistry 27*, 4915-4923.
Vermaas, W. F. J., Rutherford, A. W., & Hansson, Ö. (1988) *Proc. Natl. Acad. Sci. U.S.A. 85*, 8477-8481.
Warden, J. T., Blankenship, R. E., & Sauer, K. (1976) *Biochim. Biophys. Acta 423*, 462-478.

The Manganese Site of the Photosynthetic Oxygen-Evolving Complex Probed by EPR Spectroscopy of Oriented Photosystem II Membranes: The $g = 4$ and $g = 2$ Multiline Signals†

Dennis H. Kim,‡,§ R. David Britt,*,‖ Melvin P. Klein,*,‡ and Kenneth Sauer*,‡,§

Chemical Biodynamics Division, Lawrence Berkeley Laboratory, and Department of Chemistry, University of California, Berkeley, California 94720, and Department of Chemistry, University of California, Davis, California 95616

Received July 16, 1991; Revised Manuscript Received September 26, 1991

ABSTRACT: The $g = 4$ and $g = 2$ multiline EPR signals arising from the Mn cluster of the photosynthetic oxygen-evolving complex (OEC) in the S_2 state were studied in preparations of oriented photosystem II (PSII) membranes. The ammonia-modified forms of these two signals were also examined. The $g = 4$ signal obtained in oriented PSII membranes treated with NH_4Cl at pH 7.5 displays at least 16 partially resolved Mn hyperfine transitions with a regular spacing of 36 G [Kim, D. H., Britt, R. D., Klein, M. P., & Sauer, K. (1990) *J. Am. Chem. Soc. 112*, 9389-9391]. The observation of this $g = 4$ "multiline signal" provides strong spectral evidence for a tetranuclear Mn origin for the $g = 4$ signal and is strongly suggestive of a model in which different spin state configurations of a single exchange-coupled Mn cluster give rise to the $g = 4$ and $g = 2$ multiline signals. A simulation shows the observed spectrum to be consistent with an $S = 3/2$ or $S = 5/2$ state of a tetranuclear Mn complex. The resolution of hyperfine structure on the NH_3-modified $g = 4$ signal is strongly dependent on sample orientation, with no resolved hyperfine structure when the membrane normal is oriented perpendicular to the applied magnetic field. The dramatic NH_3-induced changes in the $g = 4$ signal resolved in the spectra of oriented samples are suggestive that NH_3 binding at the Cl^- site of the OEC may represent direct coordination of NH_3 to the Mn cluster. Orientation dependence data on the $g = 2$ multiline signal show that the hyperfine transitions in the wings of the signal are anisotropic. These peaks remain unresolved in the powder spectrum of the $g = 2$ multiline signal. The g tensor for the $g = 2$ multiline signal may be more anisotropic than previously thought.

The process of plant and cyanobacterial photosynthesis is coupled to the oxidation of water by the photosystem II (PSII)[1] reaction center complex. Four consecutive photoinduced one-electron charge separations in the PSII reaction center core are coupled to the four-electron oxidation of water by a Mn-containing enzyme, the oxygen-evolving complex (OEC). The OEC cycles through five intermediate catalytic states, designated S_0 through S_4; the conversion of S_4 to S_0 is accompanied by the release of O_2 (Kok et al., 1970). Four Mn atoms are associated with each PSII reaction center (Yocum et al., 1981) and form the active site of the OEC. The structure of the Mn site and the roles of the cofactors Ca^{2+} and Cl^-, both essential for oxygen evolution activity, have been a topic of intensive investigation [reviewed in Rutherford (1989), Sauer et al. (1991), and Debus (1991)].

Electron paramagnetic resonance (EPR) spectroscopy has been a powerful method for probing the structure of the OEC. Two EPR signals have been assigned to the Mn site of the OEC in the S_2 state. The $g = 2$ multiline signal displays at least 18 well-resolved Mn hyperfine transitions, providing direct spectroscopic evidence for the existence of an exchange-coupled Mn cluster of at least two Mn atoms (Dismukes & Siderer, 1981; Hansson & Andréasson, 1982). The second signal associated with the Mn site of the OEC in the S_2 state is centered at $g \approx 4$, has a peak-to-peak width of 300-400 G, and lacks resolved hyperfine features in PSII membranes prepared without ammonia treatment (Casey & Sauer, 1984; Zimmermann & Rutherford, 1984, 1986; Cole et al., 1987). We recently reported the observation of at least 16 Mn hyperfine transitions with a regular spacing of 36 G on the $g =$

† Supported by a grant from the National Science Foundation (DMB-8804526) and by the Director, Office of Energy Research, Office of Basic Energy Sciences, Division of Energy Biosciences of the U.S. Department of Energy, under Contract DE-AC03-76SF00098. D.H.K. gratefully acknowledges the receipt of a University of California President's Undergraduate Fellowship (1989-1990). R.D.B. gratefully acknowledges support from the Camille and Henry Dreyfus Foundation.

* Corresponding authors.
‡ Lawrence Berkeley Laboratory.
§ Department of Chemistry, University of California, Berkeley.
‖ Department of Chemistry, University of California, Davis.

[1] Abbreviations: PSII, photosystem II; OEC, oxygen-evolving complex; EPR, electron paramagnetic resonance; ESEEM, electron spin-echo envelope modulation; MES, 2-(*N*-morpholino)ethanesulfonic acid; HEPES, *N*-(2-hydroxyethyl)piperazine-*N*'-2-ethanesulfonic acid; EDTA, ethylenediaminetetraacetic acid; Chl, chlorophyll; PPBQ, phenyl-*p*-benzoquinone; Q_A, primary quinone electron acceptor in PSII.

0006-2960/92/0431-541$03.00/0 © 1992 American Chemical Society